

Supporting Information

Valorizing Natural-Abundant Glucose to Lactic Acid Using MOF-808 Catalyst under Green Hydrothermal Conditions

*Sininat Boonmark,^a Panyapat Ponchai,^a Kanyaporn Adpakpang,^a Suttipong Wannapaiboon,^b
Sutarat Thongratkaew,^c Kajornsak Faungnawakij,^c and Sareeya Bureekaew^{*a}*

^a School of Energy Science and Engineering, Vidyasirimedhi Institute of Science and Technology, 555
Moo 1 Payupnai, Wangchan, Rayong 21210, Thailand.

^b Synchrotron Light Research Institute, 111 University Avenue, Muang, Nakhon Ratchasima 30000,
Thailand.

^c National Nanotechnology Center (NANOTEC), National Science and Technology Development Agency
(NSTDA), 111 Thailand Science Park, Pahonyothin Rd., Klong Luang, Pathumthani 12120, Thailand.

Synthesis of MOF-808 and MOF-808*

As-synthesized MOF-808 was prepared based on the hydrothermal method by following the procedure reported in the literature.¹ Typically, a mixture of benzene-1,3,5-tricarboxylic acid (or trimesic acid, H₃BTC, Sigma-Aldrich) and ZrOCl₂·8H₂O (Sigma-Aldrich) was dissolved in 20 mL of 35% (v/v) of acetic acid (AA) solution. The resulting mixture was subsequently poured into a 100 mL Teflon-lined stainless-steel autoclave, then heated at 95 °C for 5 h and continuously stirred with a stirring rate of 300 rpm. The obtained white powder was centrifugated (4000 rpm, 20 min) and consecutively washed twice by aqueous sodium acetate solution (15 mL, 0.1 M) following by DI water (15 mL) and acetone (15 mL), respectively. The product was then dried in a vacuum oven at room temperature for 24 hours, resulting in MOF-808. To remove the coordinated AA, the obtained MOF-808 was activated using microwave method. 200 mg of the as-synthesized MOF-808 powder was dispersed in 7 mL of DI water and at 150 °C for 20 minutes in the microwave reactor (CEM Discovery) under vigorous stirring. After cooling to room temperature, the solid was separated out and washed with DI water and acetone for three times.² After that the powder was dried in a vacuum oven at room temperature for 24 hours to obtain the activated MOF-808 denoted as MOF-808*.

Synthesis of UiO-66

A mixture of 0.159 g zirconium (IV) chloride (ZrCl₄, Sigma-Aldrich) and 0.102 g of 1,4-benzenedicarboxylic acid (H₂BDC, Sigma-Aldrich) were dissolved in 25 mL of N, N-dimethylformamide (DMF, Daejung). The resulting mixture was poured into a 100 mL screw-cap bottle and then heated at 120 °C for 24 hours in an oven. The white powder was obtained and separated by centrifugation. The precipitate was consecutively washed with DMF and ethanol three times each. The product was then dried in a vacuum oven at room temperature for 12 hours, resulting in the as-synthesized UiO-66.³ To get rid of the coordinated DMF, the as-synthesized product was refluxed with 100 mL of DI water at 120 °C for 3 hours. After refluxing for three cycles, the product was washed with water and dried in a vacuum oven. The final product was denoted as UiO-66*.

Characterization

The crystallinity of the synthesized samples was examined using powder X-ray diffraction (PXRD) analysis (Cu K α radiation ($\lambda = 1.5406 \text{ \AA}$), Bruker, New D8 Advance). To investigate the weight-loss profiles of the samples, thermogravimetric analysis (TGA) was performed under N₂ atmosphere at the

flow rate of 200 cm³ min⁻¹ with the ramping rate of 10 °C min⁻¹ by using Rigaku thermal plus evo2 (TG 8121). Proton nuclear magnetic resonance (1H NMR) spectroscopic measurements were performed on a Bruker Avance III NMR spectrometer operating at a resonance frequency of 600.13 MHz. Each sample was weighed about 70 mg, which was digested by NaOH and added into an NMR tube containing 0.7 mL D₂O. The particle size and morphology were analyzed with a field-emission scanning electron microscope (FE-SEM, JEOL, JSM-7610F). Particle size distribution of all samples was estimated from SEM images over 200 sampling particles by using ImageJ software.⁴ The accessible active sites were probed by pyridine-adsorbed diffuse reflectance infrared Fourier transform spectroscopy (Pyridine-DRIFTS; Nicolet iS50 Spectrometer). Nitrogen (N₂) adsorption desorption isotherms were recorded at 77 K using Bel-Max sorption analyzer. Before the measurements, the samples were activated at 120 °C under reduced pressure for overnight to eliminate all guest molecules. Distributions were derived by fitting the N₂ isotherms with sets of calculated isotherms (kernel) derived from Grand Canonical Monte Carlo (GCMC) based methods. Fitting was done via the BelMaster Software Version 7.2.0.4 using a kernel for cylindrical pores provided with the software. An elemental analysis was carried out to determine the quantitative amounts of carbon in samples by the CHNS-932 model of the LECO.

Catalytic activity measurements

The lactic acid (LA) production was conducted in the 80 ml Teflon-lined stainless-steel autoclave reactor equipped with a thermocouple. The precursor solution was prepared by dissolving 0.54 g of glucose in 30 ml of DI water and transferred into the reactor. Then, 0.20 g of catalyst was added and performed the sugar conversion reaction in an inert atmosphere (N₂, 5 bar). The reaction conditions were varied to find out the optimal condition. After the reaction, the reactor was rapidly cooled down to room temperature in an ice-water bath. The liquid phase was filtered prior to analysis by high-performance liquid chromatography (HPLC, Shimadzu) equipped with both a UV detector adjusted to 210 nm and a refractive index (RI) detector using Hipler-H column (300 mm in length with a 7.7 mm i.d.; Agilent Technologies, USA). The column temperature was set to 45 °C. The samples were eluted by 8.5 mM sulfuric acid at the constant flow rate of 0.6 mL min⁻¹. The catalyst performances were evaluated in terms of glucose conversion calculated based on a molar basis as follows:

$$\text{Conversion (mol \%)} = \left(\frac{[\text{Glucose}]_{\text{initial}} - [\text{Glucose}]_{\text{final}}}{[\text{Glucose}]_{\text{initial}}} \right) \times 100$$

$$^a\text{LA Yield (mol \%)} = \left(\frac{[\text{Mole of LA}]}{[\text{Mole of Glucose}_{\text{initial}}]} \times \frac{\mathbf{1}}{\mathbf{2}} \right) \times 100$$

$$\text{5-HMF Yield (mol \%)} = \left(\frac{[\text{Mole of 5 - HMF}]}{[\text{Mole of Glucose}_{\text{initial}}]} \right) \times 100$$

$$\text{Fructose yield (mol \%)} = \left(\frac{[\text{Mole of fructose}]}{[\text{Mole of Glucose}_{\text{initial}}]} \right) \times 100$$

^a The LA yield was calculated based on a carbon-basis. Ideally, 2 moles of LA can be formed from one mole of glucose.

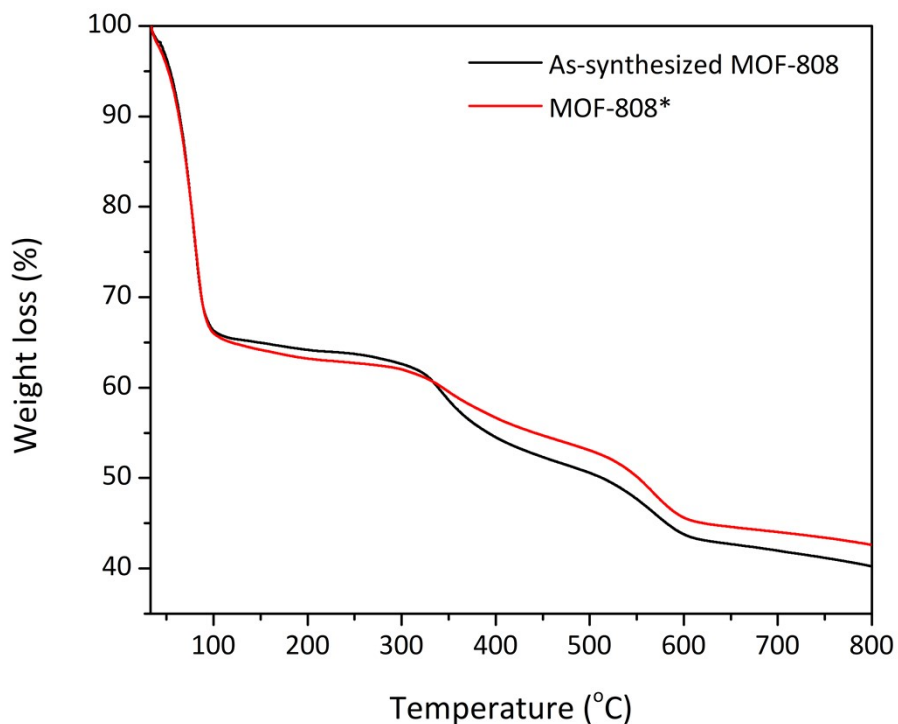


Figure S1. Thermal gravimetric analysis (TGA) curve of the as-synthesized MOF-808 and MOF-808* under N₂ at the ramping rate of 10 °C min⁻¹.

: The TGA curve of MOF-808 exhibits three prominent weight loss steps. The initial weight loss upto 100 °C is attributed to the elimination of pore-accommodated water, followed by the loss of water coordinated with open metal sites (OMSs) at 100-300 °C. This suggests that the formation of Lewis acid sites, responsible for the active sites in the reaction. Greater weight loss in this region of MOF-808* corresponds with the higher amount of OMSs, resulting in superior catalytic performance to the as-synthesized MOF-808. Subsequent weight loss at higher temperatures (300-650 °C) suggests the decomposition of the MOF-808 framework and/or the organic ligands. According to the maintained PXRD pattern of the used catalyst (Figure S7), the increased OMSs in MOF-808* do not affect the structural stability upon the reaction.

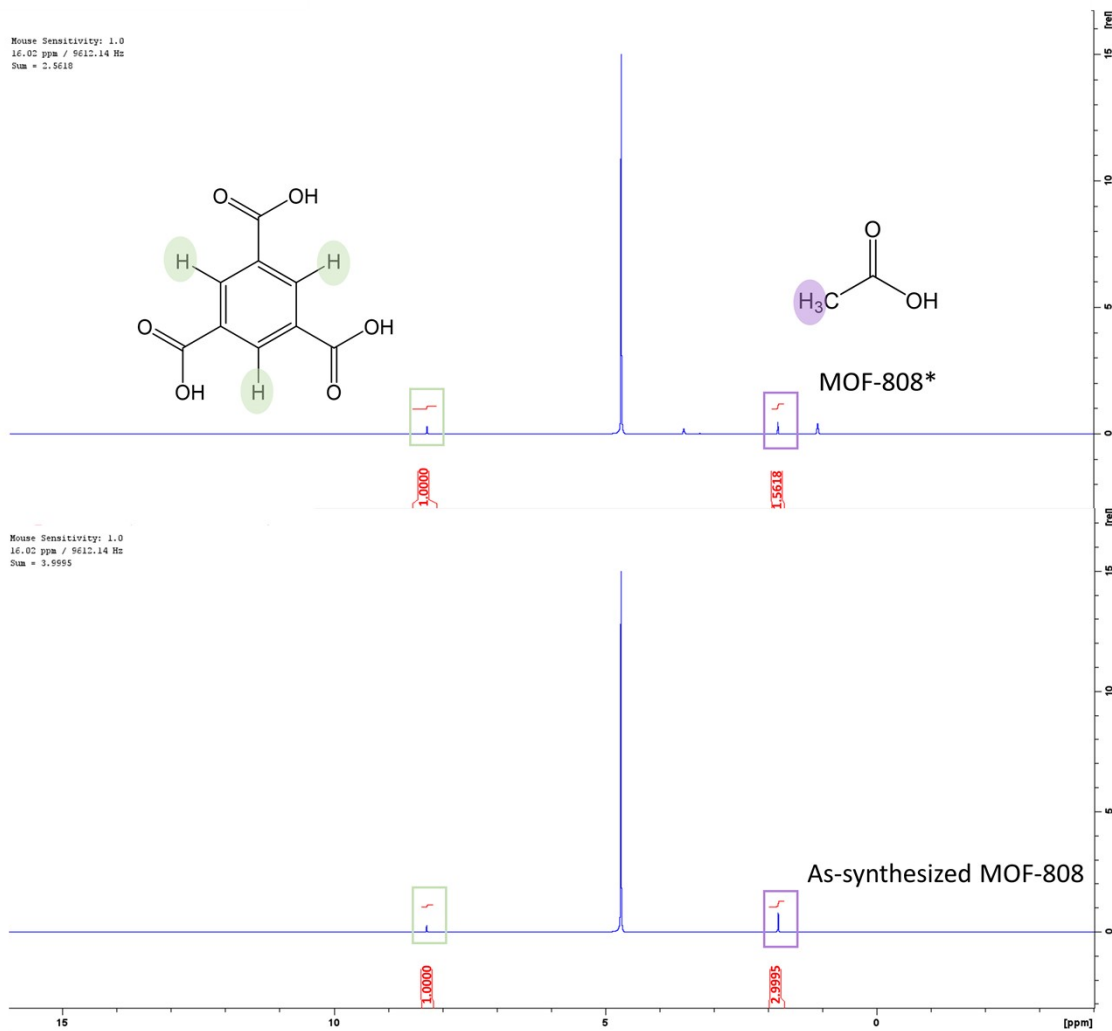


Figure S2. NMR spectra of the as-synthesized MOF-808 and MOF-808* in D₂O solvent digested by NaOH.

$$\frac{AA}{BTC} = \left(\frac{AA \text{ 1H int.}}{N_{H_{AA}}} \right) \times \left(\frac{N_{H_{BTC}}}{BTC \text{ 1H int.}} \right) = \left(\frac{AA \text{ 1H int.}}{3} \right) \times \left(\frac{3}{BTC \text{ 1H int.}} \right)$$

Table S1. Summary of molar ratio of AA: BTC in the MOF-808 catalysts.

Sample	AA ¹ H int.	BTC ¹ H int.	AA: BTC
As-synthesized MOF-808	0.999	0.333	2.998
MOF-808*	0.521	0.333	1.578

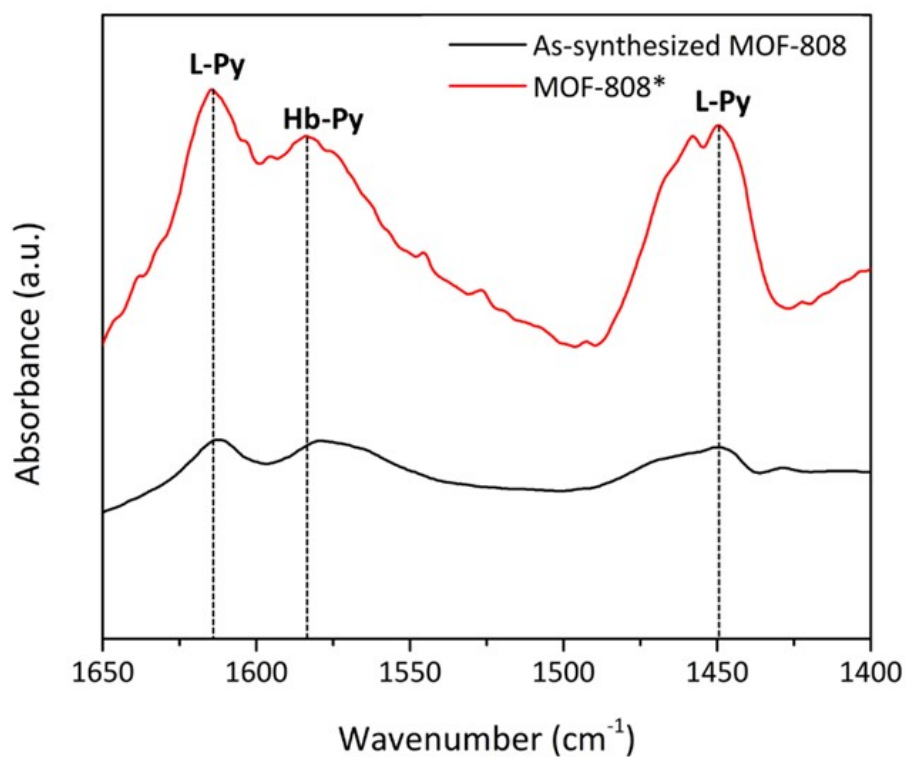


Figure S3. DRIFTS spectra of absorbed pyridine on the as-synthesized MOF-808 and MOF-808*.

: The presence of Lewis acid sites in as-synthesized MOF-808 and MOF-808* catalysts were examined through pyridine-DRIFTS analysis. The peaks at 1450 and 1615 cm^{-1} , indicate that the interaction between pyridine and Lewis acid sites (denoted as L-Py),³ are much more pronounced in activated MOF-808* compared to as-synthesized MOF-808. This confirms the higher amount of catalytic sites for glucose conversion to lactic acid. Additionally, both samples exhibit peaks at 1580 cm^{-1} ascribing hydrogen-bonded Py (denoted as Hb-Py). The more intense peak found in MOF-808* could be due to the hydrogen-bonded interaction of pyridine with -OH on active sites.

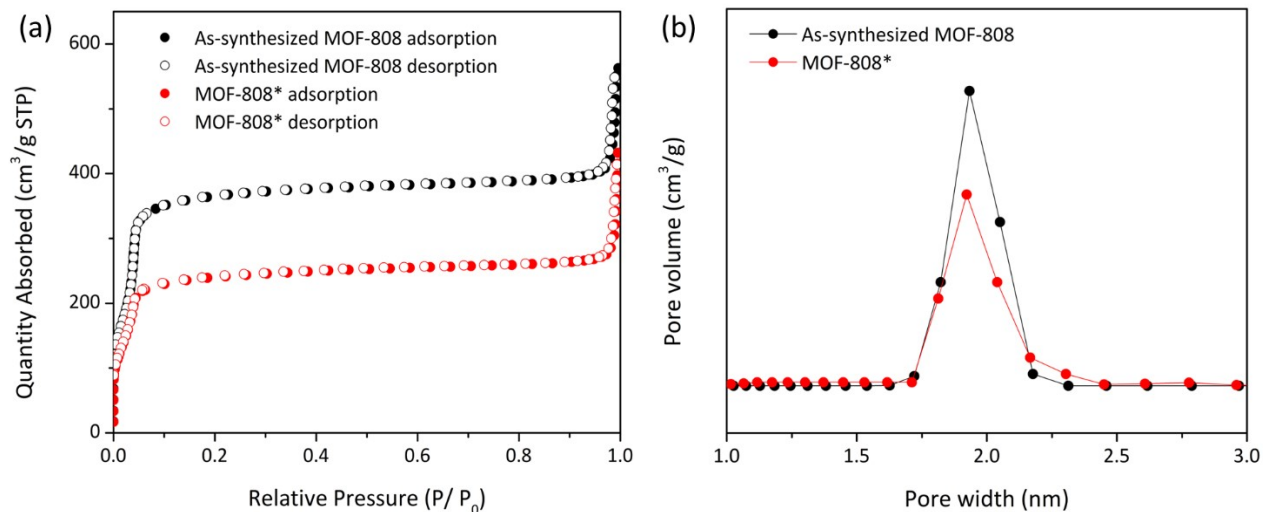


Figure S4. (a) N_2 sorption isotherms and (b) pore size distribution of the as-synthesized MOF-808 and MOF-808* measured at 77 K.

Table S2. Summary of N_2 sorption capacities of the as-synthesized MOF-808 and MOF-808* measured at 77 K. Their surface areas and pore volumes were calculated based on the Brunauer–Emmett–Teller (BET) and t-plot analysis, respectively.

Sample	Specific surface area ($m^2 g^{-1}$)	Total pore volume ($cm^3 g^{-1}$)
As-synthesized MOF-808	1414.8	0.761
MOF-808*	1047.2	0.499

: N_2 adsorption-desorption isotherms collected on the MOF-808 indicate a decrease in surface area after activation (from 1414.8 to 1047.2 $m^2 g^{-1}$ for as-synthesized MOF-808 and MOF-808*, respectively), suggesting a partial loss of framework crystallinity. However, this does not affect the catalytic performance of MOF-808*. The approximate cavities of MOF-808 and MOF-808* are similar, with a width of approximately 19.0 Å. Possessing this pore size, both MOF-808 and MOF-808* should serve as suitable platforms to accommodate glucose (8.6 Å),⁵ enabling the reaction to occur inside the cavity.

Table S3. Conversions and yields for catalytic conversion of glucose into LA on MOF-808* after hydrothermal reaction for 1 h at various reaction temperatures.

Entry	Reaction temperature (°C)	Glucose conversion (mol %)	Fructose (mol %)	LA (mol %)	5-HMF (mol %)
1	150	85.87 ± 0.31	7.41 ± 0.00	33.57 ± 0.03	13.12 ± 0.01
2	170	96.45 ± 0.42	0.95 ± 0.00	61.38 ± 0.04	11.34 ± 0.01
3	190	> 99.00	<i>n.d.^a</i>	76.62 ± 0.02	4.05 ± 0.01

^a*n.d.* = not detected

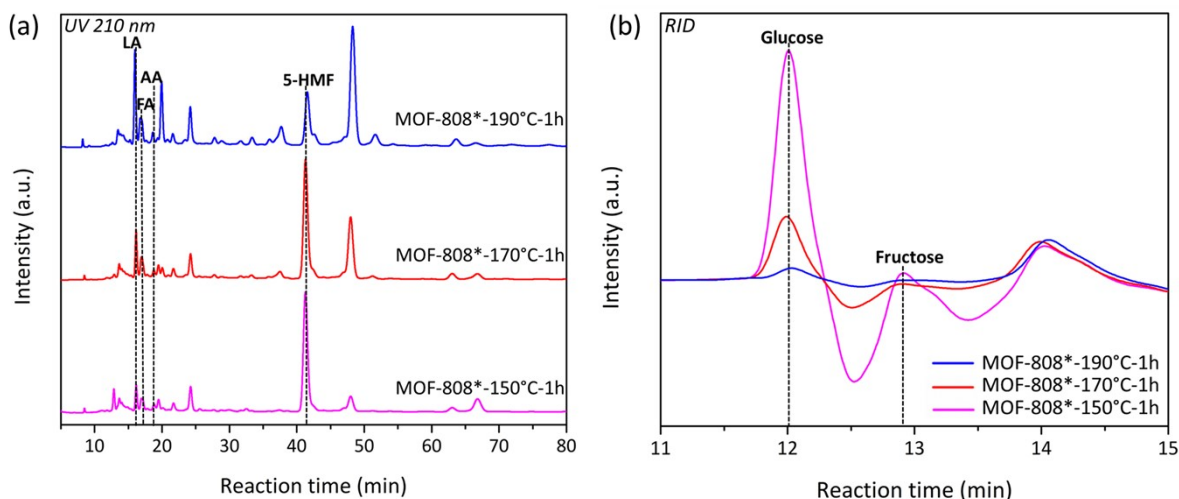


Figure S5. HPLC chromatograms from (a) UV (210 nm) and (b) RID detectors of the supernatants from the reactions employing MOF-808* as the catalyst at various temperatures for 1 h.

: This figure illustrates HPLC-UV/RID chromatograms obtained from UV (210 nm) and RID detectors of the supernatants. The UV chromatograms reveal the quantities of the resulting LA and HMF from the reaction, while the results from the RID detector provide information on glucose and fructose. At a low reaction temperature of 150 °C, while the reaction is still ongoing, a prominent fructose peak is observed (7.41 mol%) in Table S3. As the reaction temperature increases to 170 and 190 °C, only traces of the fructose peaks can be observed. These findings support the hypothesis that the MOF-808 catalyst effectively converts ketohexose glucose to aldohexose fructose before undergoing C-C bond cleavage. This suggests that the C3-C3 cleavage pathway, leading to the production of C3 LA, is the dominant route, as opposed to the C2-C4 pathway.

Table S4. Conversions and yields for catalytic conversion of glucose into LA on MOF-808* catalyst after hydrothermal reaction at 190 °C for various reaction times.

Entry	Reaction time (h)	Glucose conversion (mol %)	Fructose (mol %)	LA (mol %)	5-HMF (mol %)
1	0.5	94.13 ± 0.19	<i>n.d.</i> ^a	69.42 ± 0.01	9.01 ± 0.00
2	1	> 99.00	<i>n.d.</i>	76.62 ± 0.02	4.05 ± 0.01
3	2	> 99.00	<i>n.d.</i>	74.05 ± 0.02	1.07 ± 0.00
4	4	> 99.00	<i>n.d.</i>	52.31 ± 0.03	0.67 ± 0.01
5	6	> 99.00	<i>n.d.</i>	41.04 ± 0.01	0.09 ± 0.00

^a*n.d.*= not detected

Table S5. Conversions and yields for catalytic conversion of glucose into LA and reusability of MOF-808* catalyst after hydrothermal reaction at 190 °C for 1 h.^a

No. of reuse	Glucose conversion (mol %)	Fructose (mol %)	LA (mol %)	5-HMF (mol %)
1	> 99.00	<i>n.d.</i> ^b	76.62 ± 0.02	4.05 ± 0.01
2	97.31 ± 0.12	<i>n.d.</i>	59.89 ± 0.01	15.05 ± 0.00
3	81.20 ± 0.29	<i>n.d.</i>	42.60 ± 0.02	27.94 ± 0.00

^aThe catalyst was regenerated by washing with hot methanol. ^b*n.d.*= not detected

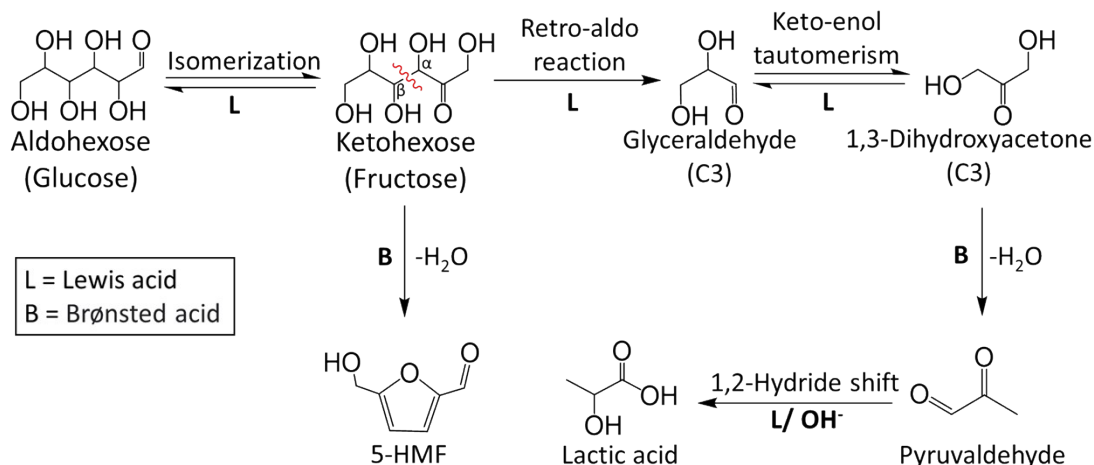
Table S6. Percentage of carbon by CHNS elemental analysis for MOF-808* catalyst before and after the glucose conversion reaction at 190 °C for 1 h.

Entry	Sample	Carbon (%)
1	MOF-808*	15.17 ± 0.28
2	MOF-808*_1 st	27.54 ± 0.19
3	MOF-808*_2 nd	35.11 ± 0.31
4	MOF-808*_3 rd	39.31 ± 0.07

: The percentage of carbon content significantly increases in the spent catalysts, confirming the presence of additional carbon species (humins) within the framework. This impedes the facile diffusion of glucose into the framework, preventing it from reaching the active sites, which consequently results in a decline in catalytic performance in the subsequent runs.

Table S7. Comparisons of catalytic performance of different heterogeneous catalysts investigated for the conversion of glucose into LA under various conditions.

Catalyst	Solvent	Conditions	Conversion (mol %)	LA (mol %)	Ref.
γ -Al ₂ O ₃	MeOH	160 °C, 6 h, 5 atm Ar	> 99.00	34.00	6
Pb-Sn-beta zeolite	H ₂ O	190 °C, 2 h	> 99.00	52.00	7
Sn-Beta zeolite	H ₂ O	200 °C, 30 m, 4.0 MPa He	98.50	57.90	8
Mg-Sn-Beta zeolites	MeOH	110 °C, 1 h, 0.4 MPa N ₂	80.00	19.00	9
In-Sn-Beta zeolites	H ₂ O	190 °C, 2 h	100.00	53.00	10
Fe-Sn/Beta	MeOH	220 °C, 6 h, 2 MPa N ₂	100.00	67.00	11
ZSM-5	H ₂ O	200 °C, 30 m, 2 MPa N ₂	> 99.80	72.40	12
ZIF-8	MeOH	160°C, 20 h	98.10	19.80	13
Mg-MOF-74	MeOH	220 °C, 6 h	100.00	35.00	14
MIL-101(Fe)	H ₂ O	190°C, 2 h	70.80	25.40	15
MOF-808*	H ₂ O	190 °C, 1 h, 5 bar N ₂	> 99.00	76.62	this work
UiO-66*	H ₂ O	190 °C, 1 h, 5 bar N ₂	97.19	33.65	this work



Scheme S1. Proposed reaction mechanism for the conversion of glucose to Lactic acid.

: Glucose undergoes isomerization to fructose, leading to glyceraldehyde (C3) and 1,3-dihydroxyacetone (C3) through the cleavage of the C–C bond in a retro-aldol step. Successive dehydration and rearrangement of glyceraldehyde and 1,3-dihydroxyacetone to form the pyruvaldehyde. Subsequently, pyruvaldehyde transforms into Lactic acid via intramolecular rearrangement by 1,2-hydrate shift. The reactions are driven by Lewis acid/-OH. It should be noted that under hydrothermal reaction conditions, the presence of acid may lead to the formation of 5-HMF. This is due to the protic solvent attributed to the dehydration of glucose, which requires a Brønsted of water, which enables the donation of protons into the system. L and B represent Lewis and Brønsted acid sites, respectively.

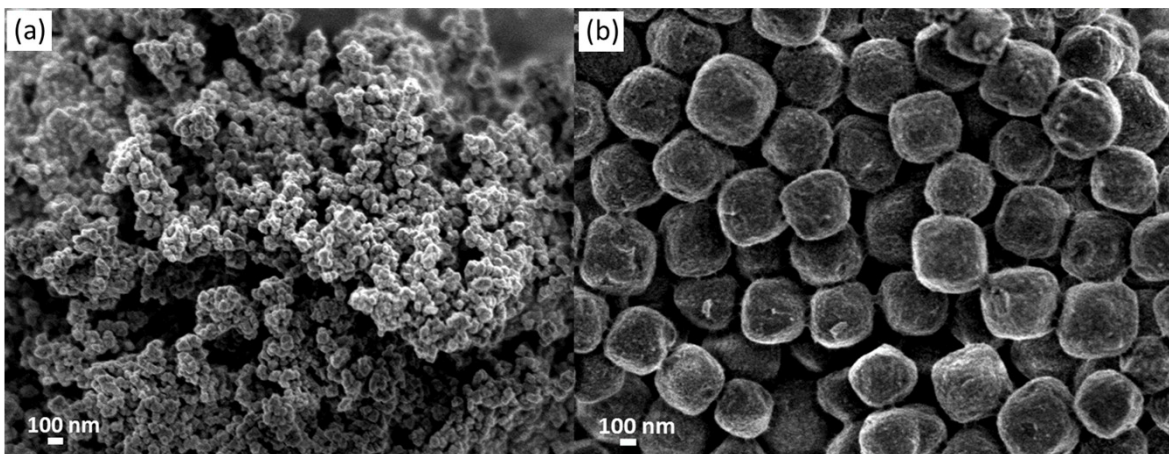


Figure S6. Scanning electron microscopic (SEM) images of (a) UiO-66* and (b) MOF-808*.

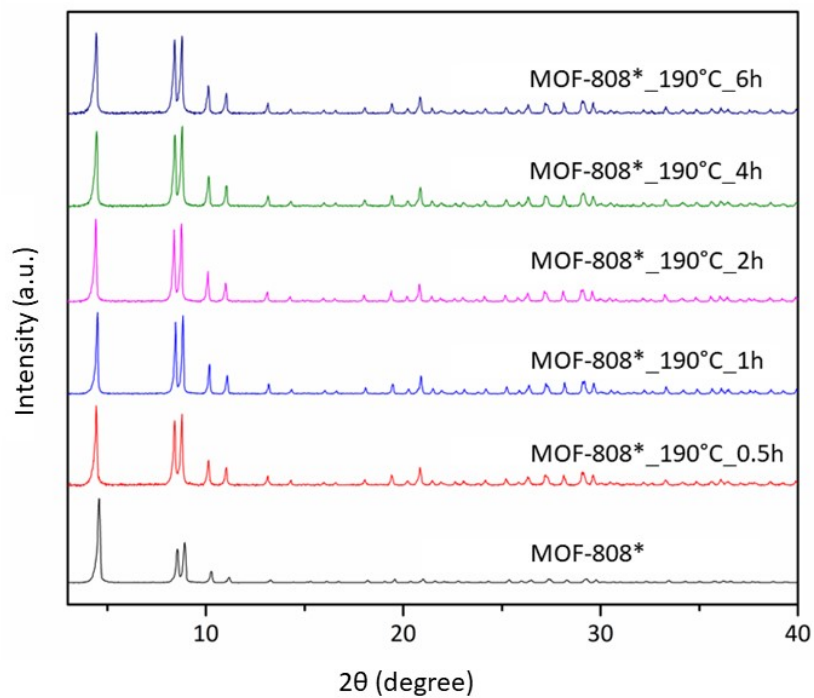


Figure S7. Powder X-ray diffraction (PXRD) patterns of the MOF-808* before and after the glucose conversion reactions at 190 °C for various reaction times.

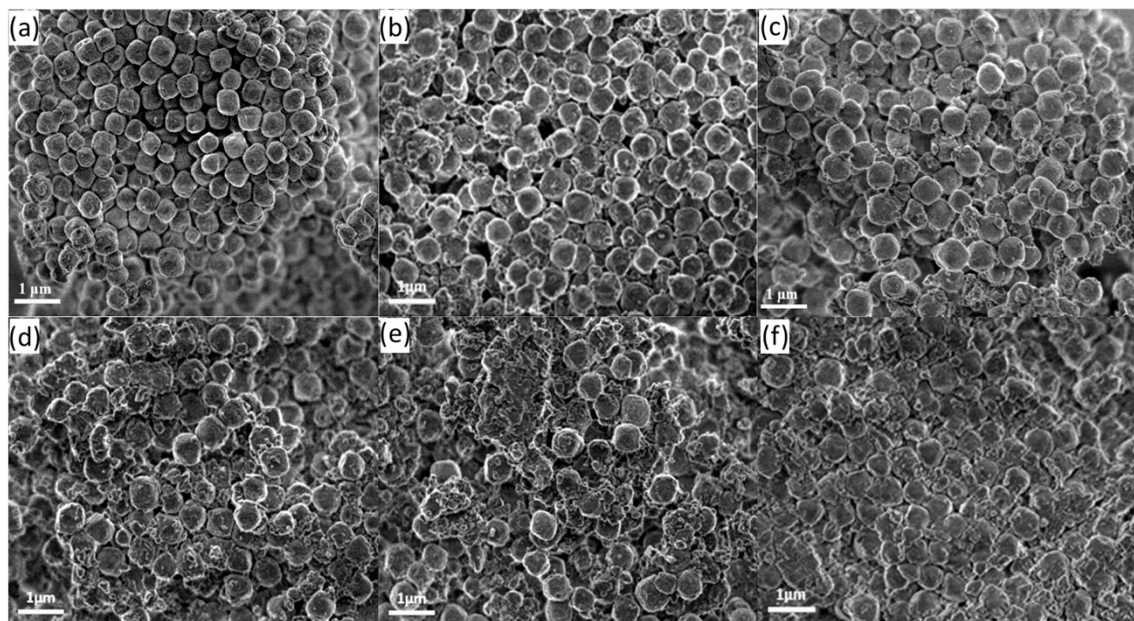


Figure S8. SEM images of MOF-808* (a) before the reaction, and after hydrothermal reactions at 190 °C for (b) 0.5 h, (c) 1 h, (d) 2 h, (e) 4 h, and (f) 6 h, respectively.



Figure S9. Photographs of MOF-808* catalyst powders (a) before the reaction, and after hydrothermal reactions at 190 °C for (b) 0.5 h, (c) 1 h, (d) 2 h, (e) 4 h, and (f) 6 h, respectively.

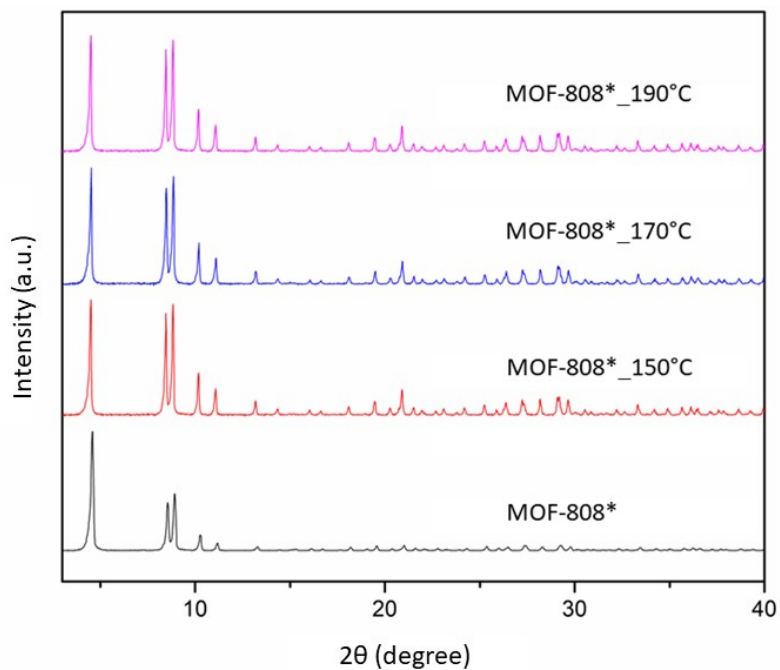


Figure S10. PXRD patterns of the MOF-808* before and after the glucose conversion reaction at various temperatures for 1 h.

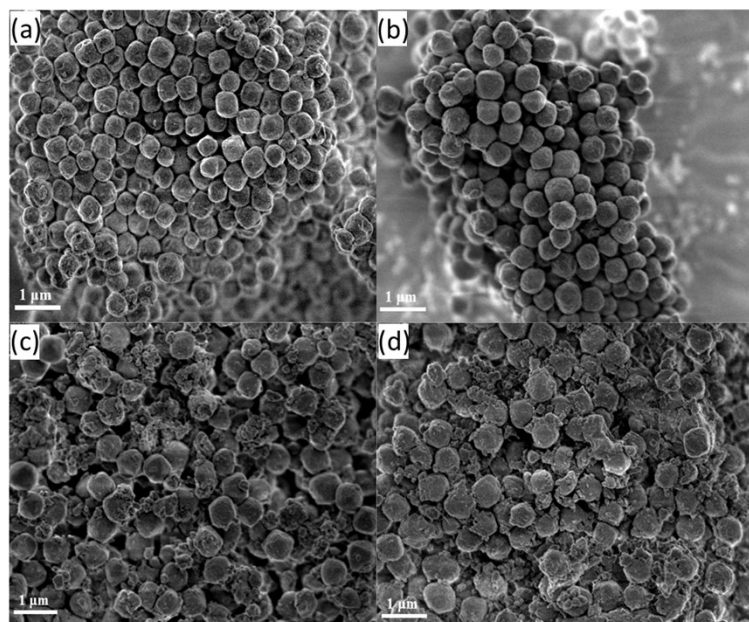


Figure S11. SEM images of MOF-808* (a) before the reaction, and after the glucose conversion reaction for 1 h at (b) 150 °C, (c) 170 °C, and (d) 190 °C, respectively.

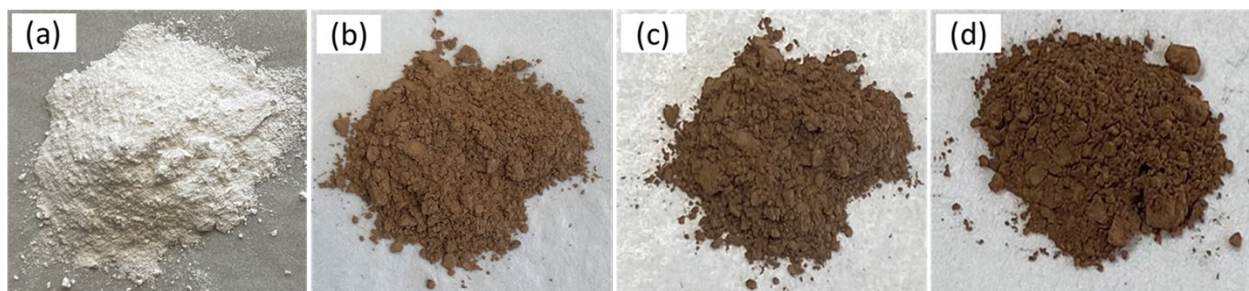


Figure S12. Photographs of MOF-808* catalyst powders (a) before the reaction, and after the glucose conversion reaction for 1 h at (b) 150 °C, (c) 170 °C, and (d) 190 °C, respectively.

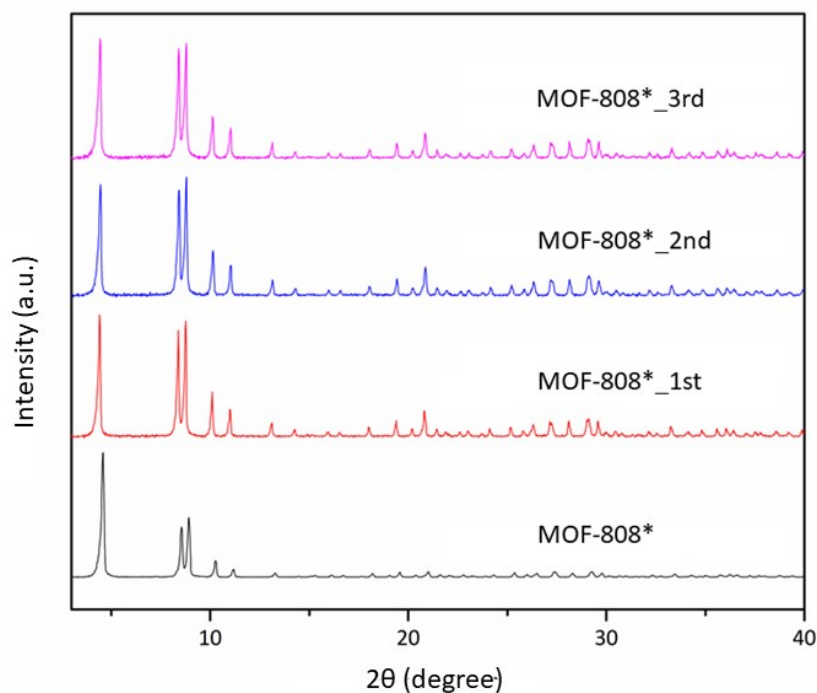


Figure S13. PXRD patterns of the MOF-808* before and after the glucose conversion reaction at 190 °C for 1 h for 3 cycles of test.

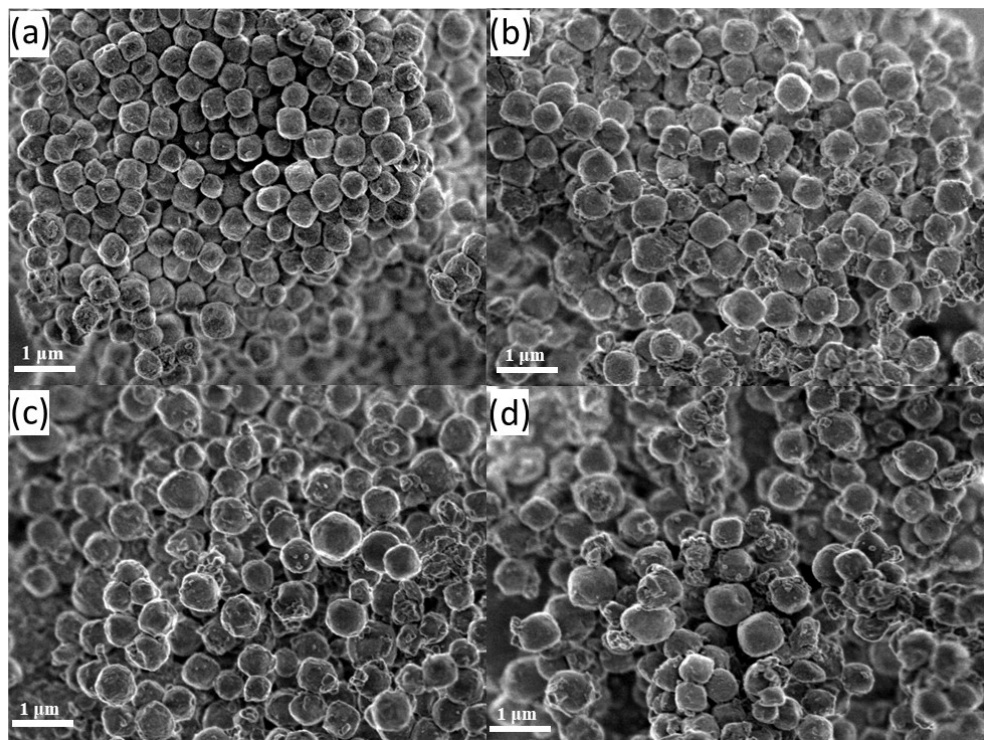


Figure S14. SEM images of MOF-808* (a) before the reaction, and after the (b) 1st, (c) 2nd, and (d) 3rd cycle of the glucose conversion reaction at 190 °C for 1 h, respectively.

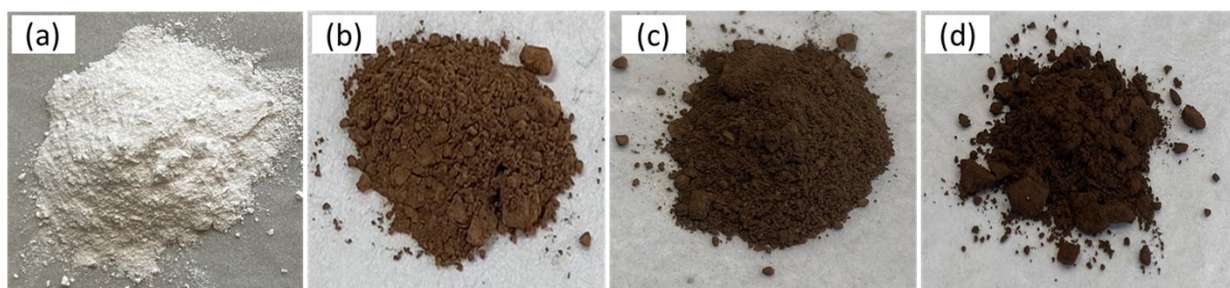


Figure S15. Photographs of MOF-808* catalyst powders after the (a) before the reaction, and after the (b) 1st, (c) 2nd, and (d) 3rd cycle of the glucose conversion reaction at 190 °C for 1 h, respectively.

References

- 1 S. Boonmark, Y. Inchongkol and S. Bureekaew, *Future Sustainable Materials through Innovation and Technology*, The 4th Material Research Society, Ubon Ratchathani, Thailand, 2023.
- 2 Y. Kalinovsky, N. J. Cooper, M. J. Main, S. J. Holder and B. A. Blight, *Dalton Trans.*, 2017, **46**, 15704-15709.
- 3 P. Ponchai, K. Adpakpang, S. Thongratkaew, K. Chaipojjana, S. Wannapaiboon, S. Siwaipram, K. Faungnawakii and S. Bureekaew, *Chem. Commun.*, 2020, **56**, 8019-8022.
- 4 C. A. Schneider, W. S. Rasband and K. W. Eliceiri, *Nat. Methods.*, 2012, **9**, 671-675.
- 5 S. Li, V. A. Tuan, J. L. Falconer and R. D. Noble, *J. Membr. Sci.*, 2001, **191**, 53-59.
- 6 S. Yamaguchi, M. Yabushita, M. Kim, J. Hirayama, K. Motokura, A. Fukuoka and K. Nakajima, *ACS Sustain. Chem. Eng.*, 2018, **6**, 8113-8117.
- 7 M. Xia, W. Dong, M. Gu, C. Chang, Z. Shen and Y. Zhang, *RSC Adv.*, 2018, **8**, 8965-8975.
- 8 Y. Sun, L. Shi, H. Wang, G. Miao, L. Kong, S. Li and Y. Sun, *Sustain. Energy Fuels*, 2019, **3**, 1163-1171.
- 9 X. Yang, B. Lv, T. Lu, Y. Su and L. Zhou, *Catal. Sci. Technol.*, 2020, **10**, 700-709.
- 10 M. Xia, W. Dong, Z. Shen, S. Xiao, W. Chen, M. Gu and Y. Zhang, *Sustain. Energy Fuels*, 2020, **4**, 5327-5338.
- 11 Q. Cai, X. Yue and W. S. Dong, *J. Porous Mater.*, 2021, **28**, 1315-1324.
- 12 Y. Xiao, S. Liao, S. Xu, J. Li, Z. Lu and C. Hu, *Renew. Energy*, 2022, **187**, 551-560.
- 13 B. Murillo, B. Zornoza, O. de la Iglesia, C. Téllez and J. Coronas, *J. Catal.*, 2016, **334**, 60-67.
- 14 X. Lu, L. Wang and X. Lu, *Catal. Commun.*, 2018, **110**, 23-27.
- 15 X. Liu, Z. Liu, Q. Zhang, H. Wu and R. Wang, *J. Chem.*, 2020, **2020**, 1-7.